

Random Wandering Around Homoclinic-like Manifolds in Symplectic Map Chain

Shin-itiro Goto* , Kazuhiro Nozaki and Hiroyasu Yamada
Department of Physics, Nagoya University, Nagoya 464-8602, Japan

Abstract

We present a method to construct a symplecticity preserving renormalization group map of a chain of weakly nonlinear symplectic maps and obtain a general reduced symplectic map describing its long-time behaviour. It is found that the modulational instability in the reduced map triggers random wandering of orbits around some homoclinic-like manifolds, which is understood as the Bernoulli shifts.

*e-mail: sgoto@allegro.phys.nagoya-u.ac.jp

1 Introduction

Hamiltonian systems with more than one degree of freedom can exhibit trajectories with complex behavior. Discrete symplectic maps are of interest since the Poincaré surface of section leads naturally to a mapping of the dynamical trajectory onto a subspace of the phase space of the Hamiltonian flow. Symplectic maps allow much easier numerical calculations of the motion than Hamiltonian flows, which are particularly convenient for studying systems of many degrees of freedom. In a two-dimensional symplectic mapping, which corresponds to Poincaré mapping of continuous-time Hamiltonian systems with two degrees of freedom, the main ingredients of this chaotic motion are hyperbolic type orbits and their invariant manifolds. The existence of transversal intersection between stable and unstable manifolds leads to non integrability of Hamiltonian systems. The area of the lobe enclosed by stable and unstable manifolds represents the flux from inside (*resp.* outside) the separatrix to outside (*resp.* inside). The manifolds which have codimension one separate the space into disjoint regions.

For symplectic mappings of four or more dimensions, there are some studies about the homoclinic bifurcation near fully hyperbolic fixed points [1][2][3]. Although the dimension of unstable and stable manifolds of a fully hyperbolic fixed point takes a maximum possible value, the transversal intersection occurs on a nearly one-dimensional homoclinic submanifold and exponentially small splitting of the homoclinic manifold leads to very weak chaos, which is almost invisible through naive numerical experiments.

A chain of weakly coupled nonlinear oscillators may present a model for dynamics near a fully elliptic fixed point. The equilibrium state of almost independent oscillators corresponds to an fully elliptic fixed point in the phase space and periodic orbits or tori encircle the elliptic fixed point. Resonant tori may be disrupted by the well-known resonance mechanism. If a torus is hyperbolic, unstable and stable manifolds attach to the torus as a “whisker” [4]. Some dynamics of such whiskers attached to tori is studied near the resonance junction by means of the naive averaging method [5].

In the case of a chain of weakly coupled nonlinear oscillators, where both coupling and nonlinearity are weak, tori may be destabilized by another mechanism called the modulational instability. Here, we study about such modulationally unstable tori and their unstable manifolds. We start with a chain of symplectic maps, each of which represents a weakly nonlinear oscillator. In order to avoid special dependence of results on the specific

form of nonlinearity, our investigation is focused on long-time asymptotic behavior of dynamics of the system. However, the conventional asymptotic methods such as the averaging method or the method of the multiple-time scales may not be immediately applicable to discrete systems. Instead, we employ the perturbative renormalization group (RG) method [6][7], which can apply to a discrete system and leads to a reduced map as the RG map [8]. However, a naive reduced map does not preserve symplectic symmetry and fails to describe long time behavior of the original symplectic map. For two-dimensional maps or special four-dimensional maps, the symplecticity is recovered through a simple “regularization” procedure [9]. For higher dimensional symplectic maps, we do not have a general procedure of “regularization”. The first purpose of this paper is to develop a general procedure of “regularization” of the RG map for a higher dimensional symplectic map. Our regularization procedure is based on the symplectic integration method for a continuous Hamiltonian flow and includes the previous regularization procedure as a special case. By means of this regularization procedure, we can derive a reduced symplectic map as the RG map, which asymptotically approximates a chain of weakly nonlinear symplectic maps.

The reduced map obtained here is general in the similar sense that the nonlinear Schrödinger equation asymptotically describes a general weakly nonlinear dispersive wave. In fact, the reduced map is found to be a space-time discrete version of nonlinear Schrödinger equation. Since the reduced map is not integrable, while its continuous limit is integrable, it is worth studying chaotic solutions of the reduced map, which is the second purpose of this paper. The reduced map has a periodic solution, which is destabilized by modulational perturbation under some conditions (the modulational instability). Then, the periodic solution becomes hyperbolic and is associated with unstable and stable manifolds, whose transversal intersection is the origin of chaos (the homoclinic chaos). It should be mentioned that various discrete versions of the nonlinear Schrödinger equation are studied in connection with numerically induced chaos of the nonlinear Schrödinger equation [10][11]. There, the systems of a large degrees of freedom are investigated in connection with numerical integration of the nonlinear Schrödinger equation and only few attentions are directed to behavior of chaotic solutions themselves.

Here, we are mainly interesting in chaotic solutions near the onset of symplectic chaos, where the phase space of the map has a dimension higher than two. Near the onset of the homoclinic chaos, an unstable manifold is

found to be very close to a stable manifold and a homoclinic-like structure is approximately preserved. In a two-dimensional symplectic map, the homoclinic chaos close to the onset is hardly seen since a splitting distance between unstable and stable manifolds is small beyond all order of the perturbation parameter. However, in a higher dimensional map considered in this paper, the weak chaos is shown to be visualized as a random rotation of some homoclinic-like orbits, which is characterized by the Bernoulli shift.

In the section 2, some reduced maps are derived from a chain of symplectic maps as the regularized RG map. The conditions of the modulational instability in the reduced maps are presented and unstable manifolds of unstable periodic orbits are depicted in the cases of two, three and four sites in the section 3. In the section 4, a random rotation of homoclinic-like orbits is observed for three- and four- site maps, which is interpreted as the the Bernoulli shift of three or four numbers.

2 Symplectic Map Chain and Reduced Map

In this section, we consider a symplectic map chain and present a method to construct a symplecticity preserving renormalization group map (a reduced symplectic map) from the symplectic map chain.

2.1 Symplecticity Preserving Renormalization Group method

We give a method to derive a symplecticity preserving reduced map from a nonlinear symplectic map of three or more sites, which is non-integrable even in the time-continuous limit.

$$x_j^{n+1} = x_j^n + \tau p_j^{n+1}, \quad (1)$$

$$p_j^{n+1} = p_j^n + \tau \left(-\Omega^2 x_j^n + \varepsilon \left\{ \nu(x_{j+1}^n - 2x_j^n + x_{j-1}^n) - \alpha(x_j^n)^3 \right\} \right), \quad (2)$$

with $N(\geq 3)$ -periodic boundary condition : $(x_{j+N}^n, p_{j+N}^n) = (x_j^n, p_j^n)$. Here x_j^n and p_j^n are real canonical variables on site j at time n , while Ω, α, ν , and τ are real parameters and ε is a small perturbation parameter, $0 < \varepsilon \ll 1$. Eliminating p -variables from Eqs. (1) and (2), we obtain a map for x -variables:

$$x_j^{n+1} - 2 \cos(\theta) x_j^n - x_j^{n-1} = \varepsilon \tau^2 \left\{ \nu(x_{j+1}^n - 2x_j^n + x_{j-1}^n) - \alpha(x_j^n)^3 \right\}, \quad (3)$$

where $\cos(\theta) = (1 - \Omega^2\tau^2/2)$. Let us construct a reduced map for $0 < \varepsilon \ll 1$ by means of the RG method. Expanding a solution of Eq. (3) as $x_j^n = x_j^{n(0)} + \varepsilon x_j^{n(1)} + \mathcal{O}(\varepsilon^2)$, $j = 1, 2, \dots$, we have

$$\begin{aligned} x_j^{n(0)} &= A_j \exp(-i\theta n) + \text{c.c.}, \\ \mathcal{L}x_j^{n(1)} &= \tau^2 \left\{ \nu \Delta_j^2 A_j - 3\alpha |A_j|^2 A_j \right\} \exp(-i\theta n) + \text{c.c.}, \end{aligned}$$

where

$$\mathcal{L}x_j^{n(1)} \equiv x_j^{n+1(1)} - 2 \cos \theta \cdot x_j^{n(1)} + x_j^{n-1(1)}, \quad (4)$$

$$\Delta_j^2 A_j^n \equiv A_{j+1}^n - 2A_j^n + A_{j-1}^n, \quad (5)$$

and c.c. denotes complex conjugate to the preceding terms; A_j is an integration constant associated with a site j . The first order solution has a secular term with respect to n .

$$x_j^{n(1)} = n \frac{i\tau^2}{2 \sin \theta} \left\{ \nu \Delta_j^2 A_j - 3\alpha |A_j|^2 A_j \right\} \exp(-i\theta n) + \text{c.c.} + \text{n.r.},$$

and n.r. denotes non-resonant terms. In order to remove this secular term, we define a renormalization transformation $A_j \mapsto A_j^n$ by

$$A_j^n \equiv A_j + \varepsilon \left\{ n \frac{i\tau^2}{2 \sin \theta} \left(\nu \Delta_j^2 A_j - 3\alpha |A_j|^2 A_j \right) \right\} + \mathcal{O}(\varepsilon^2). \quad (6)$$

A discrete version of the RG equation is constructed by taking difference of A_j^n ,

$$A_j^{n+1} - A_j^n = \varepsilon \left\{ \frac{i\tau^2}{2 \sin \theta} \left(\nu \Delta_j^2 A_j - 3\alpha |A_j|^2 A_j \right) \right\}. \quad (7)$$

Substituting the expression for A_j in terms of A_j^n defined by Eq. (6) into Eq. (7), we can eliminate the secular term up to $\mathcal{O}(\varepsilon)$ and obtain a naive RG map

$$A_j^{n+1} = A_j^n + \varepsilon \left\{ \frac{i\tau^2}{2 \sin \theta} \left(\nu \Delta_j^2 A_j^n - 3\alpha |A_j^n|^2 A_j^n \right) \right\}, \quad (8)$$

or

$$\frac{A_j^{n+1} - A_j^n}{\tau} = \varepsilon \left\{ \frac{i\tau}{2 \sin \theta} \left(\nu \Delta_j^2 A_j^n - 3\alpha |A_j^n|^2 A_j^n \right) \right\}. \quad (9)$$

This naive RG map does not preserve symplectic symmetry. To recover symplecticity of Eq. (8), we apply the symplectic integration method to the

continuous-time limit ($\tau \rightarrow 0$) of the naive RG map (9). The continuous-time limit takes the following symplectic form, which is also derived from the continuous-time limit of Eqs. (1) and (2) in the Appendix A,

$$\frac{dA_j}{dt} = i\varepsilon \frac{1}{2\Omega} \left(\nu \Delta_j^2 A_j^n - 3\alpha |A_j^n|^2 A_j^n \right) = \frac{\partial H^{RG}}{\partial A_j^*}, \quad \frac{dA_j^*}{dt} = -\frac{\partial H^{RG}}{\partial A_j}. \quad (10)$$

Here, $\Omega = \frac{\sin(\theta)}{\tau}$ as $\tau \rightarrow 0$ and H^{RG} is given by

$$\begin{aligned} H^{RG} &= H^\nu + H^\alpha, \\ H^\nu &= -\frac{i\varepsilon\nu}{2\Omega} \sum_j |A_{j+1} - A_j|^2, \\ H^\alpha &= \frac{3i\varepsilon\alpha}{4\Omega} \sum_j |A_j|^2. \end{aligned}$$

The Hamiltonian flow defined by H^α can be solved as

$$A_j(t + \tau') = A_j(t) \exp \left(-\frac{3i\varepsilon\alpha}{2\Omega} |A_j(t)|^2 \tau' \right),$$

where τ' is an arbitrary constant and we have

$$A_j^{n+1} = A_j^n \exp \left(-\frac{3i\varepsilon\alpha}{2\Omega} |A_j^n|^2 \tau \right). \quad (11)$$

The flow defined by H^ν can be discretized by the symplectic implicit midpoint rule [12]: a general Hamiltonian flow

$$\frac{dz}{dt} = f(z),$$

is discretized as

$$z^{n+1} = z^n + \tau f \left(\frac{1}{2} (z^{n+1} + z^n) \right).$$

In our case, the scheme gives

$$A_j^{n+1} = A_j^n + \tau \frac{i\varepsilon\nu}{2\Omega} \frac{1}{2} \left(\Delta_j^2 A_j^{n+1} + \Delta_j^2 A_j^n \right), \quad (12)$$

or a temporally explicit form

$$\left(1 - i\tau \frac{i\varepsilon\nu}{2\Omega} \frac{1}{2} \Delta_j^2 \right) A_j^{n+1} = \left(1 + i\tau \frac{i\varepsilon\nu}{2\Omega} \frac{1}{2} \Delta_j^2 \right) A_j^n. \quad (13)$$

Combining two symplectic transformations (11) and (13), we get a symplectic scheme for $H = H^\nu + H^\alpha$ as

$$\left(1 - i\tau \frac{i\varepsilon\nu}{2\Omega} \frac{1}{2} \Delta_j^2\right) A_j^{n+1} = \left(1 + i\tau \frac{i\varepsilon\nu}{2\Omega} \frac{1}{2} \Delta_j^2\right) \exp\left(-\frac{3i\varepsilon\alpha}{2\Omega} |A_j^n|^2 \tau\right) A_j^n.$$

For brevity, we rewrite the above symplectic RG map as

$$\left(1 - iT \Delta_j^2\right) A_j^{n+1} = \left(1 + iT \Delta_j^2\right) \exp\left(iQ |A_j^n|^2\right) A_j^n, \quad (14)$$

where

$$T \equiv \varepsilon \frac{\nu\tau^2}{4 \sin \theta} \in \mathbf{R}, \quad Q \equiv \varepsilon \frac{-3\alpha\tau^2}{2 \sin \theta} \in \mathbf{R}.$$

Which has a conserved quantity $\sum_j |A_j^n|^2$ (see Ref. [13]). Both temporally and spatially explicit form of Eq.(14) is possible. For instance, the three-site map is written as

$$\begin{pmatrix} A_1^{n+1} \\ A_2^{n+1} \\ A_3^{n+1} \end{pmatrix} = \frac{1 - 3iT}{1 + 9T^2} \begin{pmatrix} 1 - iT & 2iT & 2iT \\ 2iT & 1 - iT & 2iT \\ 2iT & 2iT & 1 - iT \end{pmatrix} \begin{pmatrix} B_1^n \\ B_2^n \\ B_3^n \end{pmatrix},$$

where

$$B_j^n \equiv \exp(iQ |A_j^n|^2) A_j^n.$$

An approximate solution of the original map (1) and (2) is expressed in terms of the renormalized amplitude as $x_j^n \approx A_j^n \exp(-i\theta n) + \text{c.c.}$ If the coupling parameter ν vanishes, the present regularization process is nothing but a simple exponentiation procedure introduced in [9]. Note that the Eq.(14) with $N \gg 1$ is identical to a difference scheme for the nonlinear Schrödinger equation [13]. In fact, the time-continuous limit of the RG map (14) is just a spatially discretized nonlinear Schrödinger equation (see Appendix A). The map (14) also admits some oscillating solutions including a spatially uniform one.

2.2 Nonlinear symplectic map with two sites

Let us consider a nonlinear symplectic map with two sites. This system is separately discussed since the continuous-time limit ($\tau \rightarrow 0$) of its RG map

is integrable.

$$x_1^{n+1} = x_1^n + \tau p_1^{n+1}, \quad x_2^{n+1} = x_2^n + \tau p_2^{n+1}, \quad (15)$$

$$p_1^{n+1} = p_1^n + \tau \left\{ -\Omega^2 x_1^n + \varepsilon \left(\nu(x_2 - x_1) - \alpha x_1^3 \right) \right\}, \quad (16)$$

$$p_2^{n+1} = p_2^n + \tau \left\{ -\Omega^2 x_2^n + \varepsilon \left(\nu(x_1 - x_2) - \alpha x_2^3 \right) \right\}. \quad (17)$$

We rewrite Eqs. (15) – (17) as follows,

$$x_1^{n+1} - 2 \cos \theta \cdot x_1^n + x_1^{n-1} = \varepsilon \tau^2 \left\{ \nu(x_2^n - x_1^n) - \alpha (x_1^n)^3 \right\},$$

$$x_2^{n+1} - 2 \cos \theta \cdot x_2^n + x_2^{n-1} = \varepsilon \tau^2 \left\{ \nu(x_1^n - x_2^n) - \alpha (x_2^n)^3 \right\},$$

where θ is defined in Eq. (3). Setting $x_j^n \approx A_j^n \exp(-i\theta n) + \text{c.c.}$ and following the same procedure as in the case of the three- or more- site model, we reach a regularized RG map up to $\mathcal{O}(\varepsilon)$

$$(1 - iTL_j)A_j^{n+1} = (1 + iTL_j) \exp(iQ|A_j^n|)A_j^n, \quad (j = 1, 2) \quad (18)$$

where an operator L_j is defined by

$$L_1 A_1^n \equiv -A_1^n + A_2^n, \quad L_2 A_2^n \equiv A_1^n - A_2^n. \quad (19)$$

The detail derivation of this regularized RG map is shown in Appendix B. It is worth noting that the map (18) has not only symplectic symmetry but also a conserved quantity

$$\sum_{j=1,2} |A_j^n|^2 = \sum_{j=1,2} |A_j^0|^2. \quad (20)$$

The map (18) has oscillating solutions

$$A_1^n = A_2 = A^0 \exp\left(iQ|A^0|^2 n\right), \quad (21)$$

or

$$A_1^n = -A_2 = A^0 \exp\left(iQ|A^0|^2 n\right), \quad (22)$$

where A^0 is a constant. The family of these solutions lies on a one-dimensional torus in the phase space that spanned by A_j^n and A_j^{n*} . The (modulational)

stability of solutions (21) and (22) is of interest because the stability determines hyperbolicity or ellipticity of the torus. If the torus is hyperbolic, unstable and stable manifolds attach to the torus like “whiskers” [4] and we call such unstable and stable manifolds whiskers in this paper.

Behavior of such whiskers is the main object to investigate in the following sections 3 and 4. Let us show effectiveness of the regularized RG map by numerical calculations. In Fig. 1, trajectories obtained from the naive RG map (8) and the regularized RG map (14) are depicted to be compared to an exact trajectory of the original map (Eqs. (1)–(2)). All initial points are set very close to a hyperbolic torus. The trajectory given by the regularized RG map is in good agreement with the exact solution.

Owing to the conserved quantity (20), the time-continuous limit ($\tau \rightarrow 0$) of the RG map (18) becomes integrable and analytical expression of whiskers, which is exactly homoclinic in this case, is given in the Appendix C.

3 Whiskered Tori

In this section, we analyze the modulational instability of spatially uniform oscillating solutions (tori) of the reduced maps derived in the previous section and introduce whiskered tori, that is, the hyperbolic structure near periodic manifolds. It is found that whiskers retain the homoclinic structure approximately near the onset of the modulational instability, where the homoclinic chaos is weak.

3.1 Two-site case

Let us analyze the reduced symplectic map with two sites, whose continuous-time limit is integrable.

One of tori of Eq. (18) is just a spatially uniform solution

$$A_j^n = A^0 \exp(iQ|A^0|^2 n), \quad (j = 1, 2).$$

To study the phase space structure around the solution, we consider a perturbed solution of the form

$$A_j^n = A^0 \exp(iQ|A^0|^2 n) \left(1 + \mu_j^n\right), \quad (23)$$

where $|\mu_j^n|^2 \ll 1$. Substitution of this expression into (18) and retaining first order terms in μ_j^n , yield

$$\begin{aligned} \begin{pmatrix} 1 + iT & -iT \\ -iT & 1 + iT \end{pmatrix} \begin{pmatrix} \mu_1^{n+1} \\ \mu_2^{n+1} \end{pmatrix} &= (1 + iQ|A^0|^2) \begin{pmatrix} 1 - iT & iT \\ iT & 1 - iT \end{pmatrix} \begin{pmatrix} \mu_1^n \\ \mu_2^n \end{pmatrix} \\ &+ iQ|A^0|^2 \begin{pmatrix} 1 - iT & iT \\ iT & 1 - iT \end{pmatrix} \begin{pmatrix} \mu_1^{n*} \\ \mu_2^{n*} \end{pmatrix} \end{aligned} \quad (24)$$

and complex conjugate to the above expression. The eigenvalues of Eqs.(24) are

$$1, \quad 1, \quad \lambda_{\pm} = \beta \pm \sqrt{\beta^2 - 1}, \quad (25)$$

where $\beta \equiv (1 - 4T^2 + 4Q|A^0|^2T)/(1 + 4T^2)$. We obtain conditions for the instability

$$|A^0|^2 > \frac{2T}{Q}, \quad (26)$$

or

$$|A^0|^2 < -\frac{1}{2QT}, \quad (27)$$

which comes from $\beta^2 > 1$. Hereafter, we concentrate on the condition (26), under which the torus becomes hyperbolic for the amplitude $|A^0|$ larger than a critical value ($\sqrt{2T/Q}$). From the spectrum of eigenvalues (25), we find that whiskers consists of one-dimensional unstable manifold (departing whisker) and one-dimensional stable manifold (arriving whisker). To construct whiskers numerically, we transform A_j^n to $a_j^n (j = 1, 2)$ where

$$A_j^n = a_j^n \exp(iQ|A^0|^2 n).$$

The torus with departing whiskers are depicted in Figs 2. Even if $|A^0|$ is considerably larger than the critical value, whiskers are found to be almost homoclinic and their behavior appears to be regular. This apparent regularity reflects the integrability of continuous-time limit of the map with two sites and is sharp contrast to the case of three or more sites as studied in the subsequent sections. Since difference between the map (18) and its integrable continuous-time limit is very small (beyond all order), the weak homoclinic chaos may be almost invisible in the present range of numerical calculations.

3.2 Three-site case

Let us consider the regularized RG map with three sites (14). When the site number is odd, general stability analysis is possible and is provided in Appendix D. Similar linearized analysis around a uniformly oscillation solution as in the previous subsection leads to instability conditions:

$$|A^0|^2 > \frac{3T}{Q}, \quad (28)$$

or

$$|A^0|^2 < \frac{-1}{3QT}. \quad (29)$$

As well as the two-site model, we consider the condition (28) only. The spectrum of the linearized map is given as

$$\begin{aligned} \lambda_a &\equiv \beta_a \pm \sqrt{\beta_a^2 - 1}, & (a = 0, 1) \\ \beta_0 &= 1, & (\text{singlet}) \\ \beta_1 &= \frac{1 + 6Q|A^0|^2T - 9T^2}{1 + 9T^2}, & (\text{doublet}), \end{aligned} \quad (30)$$

The spectrum (30) shows that the dimension of both departing and arriving whiskers are two for three-site case. The tori with its unstable manifolds are depicted in Figs. 3. These figures show that the whiskers' behavior is different from that of two-site case. The difference may be attributed to one of integrability property of their continuous-time limit. The greater is the amplitude of tori, the more complicate is the whisker's behavior. When the amplitude is just above a critical value ($\sqrt{3T/Q}$) for the instability, whiskers are found to be still homoclinic-like as shown in Fig 3 (a).

3.3 Four-site case

We analyse the modulational instability of a uniformly oscillating solution of the regularized RG map with four sites (14) separately since general analysis is possible only for the odd-site case (Appendix D).

The linearized map around a uniformly oscillating solution (a torus) has the following eight eigenvalues

$$\begin{aligned} \lambda_{a\pm} &\equiv \beta_a \pm \sqrt{\beta_a^2 - 1}, & (a = 0, 1, 2) \\ \beta_0 &= 1, & (\text{singlet}) \end{aligned}$$

$$\beta_1 = \frac{1 + 4Q|A^0|^2T - 4T^2}{1 + 4T^2}, \quad (\text{doublet})$$

$$\beta_2 = \frac{1 + 8Q|A^0|^2T - 16T^2}{1 + 16T^2}, \quad (\text{singlet}).$$

The eigenvalues give the following instability conditions of the torus.

$$|A^0|^2 > \frac{2T}{Q} \quad (\text{doublet}), \quad |A^0|^2 > \frac{4T}{Q} \quad (\text{singlet}), \quad (31)$$

or

$$|A^0|^2 < -\frac{1}{2QT} \quad (\text{doublet}), \quad |A^0|^2 < -\frac{1}{4QT} \quad (\text{singlet}), \quad (32)$$

where we consider the conditions (31) only as before. The spectrum of eigenvalues gives the dimension of whiskers associated with the torus:

- $|A^0|^2 < \frac{2T}{Q}$ \dots no whiskers (elliptic),
- $\frac{2T}{Q} < |A^0|^2 < \frac{4T}{Q}$ \dots 2 dimensional departing and 2 dim arriving whiskers and ellipticity is equal to 2 dimensions,
- $|A^0|^2 > \frac{4T}{Q}$ \dots 3 dimensional departing and 3 dimensional arriving whiskers.

The torus with its unstable manifold is depicted in Fig. 4. As similar to the three-site case, the greater is the amplitude of torus, the more complicate is whiskers' behavior.

4 Random Rotation of Homoclinic-like Orbits

For slightly above the critical amplitude, we study chaotic orbit's behavior in the three- and four-site cases. In such cases, an orbit wanders randomly around some homoclinic-like manifolds (whiskers) and it looks like a random sequence of homoclinic-like orbits as shown in Fig. 5. Each homoclinic-like orbit only differs in which site takes the largest amplitude in the orbit. In other word, a random rotation of site-numbers occurs in a sequence of

the same homoclinic-like structure. This random rotation of site-numbers is understood by means of the Bernoulli shift. Let us characterize each homoclinic-like orbit by the site-number of the largest amplitude so that an orbit is represented by a sequence of site-numbers

$$10210120 \cdots \quad (\text{resp. } 112301 \cdots), \quad \text{etc.}$$

corresponding to the sequence in Figs. 6 and 7, where 0 indicates the site number 3 or 4. This random sequence of numbers is conceived by the Bernoulli sequence, which is generated by a simple map

$$w^{n+1} = 3w^n \quad (\text{resp. } w^{n+1} = 4w^n), \quad \text{mod } 1.$$

A periodic sequence of homoclinic-like orbits corresponds to a periodic solution of the Bernoulli map for a rational initial value on the interval $[0, 1)$, while a random sequence is generated for an irrational initial value.

Now, we present some number sequences of the homoclinic-like whiskers obtained by numerical iterations of the three-site case and the four-site case respectively in Fig. 8. These figures suggest that the sequences of homoclinic-like orbits is not periodic but random. It should be noted that such a random rotation of homoclinic-like orbits does not appear in the two-site case.

5 Conclusion

We present a regularization procedure to preserve the symplectic structure of the RG map near a fully elliptic fixed point of a chain of weakly nonlinear symplectic maps. The regularization is accomplished by extended exponentiation of the naive RG map and we derive a general reduced symplectic map as an asymptotic RG map.

Analyzing the modulational instability of a uniformly oscillation solution of the reduced map, we find a hyperbolic torus with whiskers. We observe that whiskers retain a homoclinic-like structure in the case the amplitude of the uniformly oscillating solution exceeds slightly the critical value. For three or more-site cases, we find a random sequence of the homoclinic-like orbits. The orbit is symbolized by a random rotation of site-numbers generated by the Bernoulli shifts. Although this chaos may be produced by the homoclinic mechanism and is very weak, it is easily visible as a random sequence of homoclinic-like orbits. Such easily visible irregularity of homoclinic-like

orbits may be general in high-dimensional chaos and give an important visible tool to understand the onset of chaotic dynamics in high-dimensional spaces.

Acknowledgement

The present work is, in part, supported by the Japan Society for Promotion of Science, Grand-in-Aid for Scientific Research (C) 13640402.

Appendix

Appendix A: Continuous-time RG equation with three or more sites

Here, we give an RG equation of continuous-time limit ($\tau \rightarrow 0$) of the weakly nonlinear chain (1) and (2), which is a spatially discretized nonlinear Schrödinger equation. Continuous-time limit of Eqs. (1) and (2) reads

$$\begin{aligned} \frac{dx_j}{dt} &= p_j = \frac{\partial H}{\partial p_j}, \\ \frac{dp_j}{dt} &= -\Omega^2 x_j + \varepsilon \left\{ \nu (x_{j+1} - 2x_j + x_{j-1}) - \alpha x_j^3 \right\} = -\frac{\partial H}{\partial x_j}, \\ H &= \sum_l \left[\frac{p_l^2 + \Omega^2 x_l^2}{2} + \varepsilon \alpha \frac{x_l^4}{4} \right] + \sum_l \varepsilon \nu \left[\frac{(x_{l+1} - x_l)^2}{2} \right]. \end{aligned}$$

Expanding x_j as $x_j = x_j^{(0)} + \varepsilon x_j^{(1)} + \mathcal{O}(\varepsilon^2)$, a naive perturbed solution is obtained as

$$\begin{aligned} x_j^{(0)} &= A_j \exp(-i\Omega t) + \text{c.c.} \\ x_j^{(1)} &= \frac{it}{2\Omega} \left(\nu \Delta_j^2 A_j - 3\alpha |A_j|^2 A_j \right) \exp(-i\Omega t) + \text{c.c.} + \text{n.r.}, \end{aligned}$$

where A_j is a complex valued integration constant for j -th site. To remove secular terms proportional to t , we define the renormalization transformation $A_j \mapsto \tilde{A}_j(t)$ by collecting all terms proportional to the fundamental harmonic $\exp(-i\Omega t)$

$$\tilde{A}_j(t) \equiv A_j + \varepsilon \frac{it}{2\Omega} \left(\nu \Delta_j^2 A_j - 3\alpha |A_j|^2 A_j \right) + \mathcal{O}(\varepsilon^2),$$

From this transformation, the prescription of the RG method [7] gives an RG equation

$$\frac{d\tilde{A}_j}{dt} = i\varepsilon \frac{1}{2\Omega} \left(\nu \Delta_j^2 \tilde{A}_j - 3\alpha |\tilde{A}_j|^2 \tilde{A}_j \right). \quad (33)$$

This RG equation automatically retains the symplectic property and is known as a spatially discretised nonlinear Schrödinger equation, which is also non-integrable except the case of two sites.

Appendix B: Derivation of a reduced map of two-site nonlinear symplectic map

In this subsection, we derive a regularized RG map from a nonlinear two-site symplectic map chain.

Expanding x_1^n and x_2^n as $x_j^n = x_j^{n(0)} + \varepsilon x_j^{n(1)} + \mathcal{O}(\varepsilon^2)$, ($j = 1, 2$), we have the following naive perturbative solution of Eqs. (15) – (17)

$$\begin{aligned} x_j^{n(0)} &= A_j \exp(-i\theta n) + \text{c.c.}, \\ x_1^{n(1)} &= \tau^2 \left\{ \nu(A_2 - A_1) - 3\alpha |A_1|^2 A_1 \right\} \exp(-i\theta n) + \text{c.c.} + \text{n.r.}, \\ x_2^{n(1)} &= \tau^2 \left\{ \nu(A_1 - A_2) - 3\alpha |A_2|^2 A_2 \right\} \exp(-i\theta n) + \text{c.c.} + \text{n.r.} \end{aligned}$$

The renormalization transformation $A_j \mapsto A_j^n$ to remove the secular terms in the coefficient of $\exp(-i\theta n)$ is given by

$$\begin{aligned} A_1^n &\equiv A_1 + \varepsilon n \frac{i\tau^2}{2 \sin \theta} \left\{ \nu(A_2 - A_1) - 3\alpha |A_1|^2 A_1 \right\} + \mathcal{O}(\varepsilon^2) \\ A_2^n &\equiv A_2 + \varepsilon n \frac{i\tau^2}{2 \sin \theta} \left\{ \nu(A_1 - A_2) - 3\alpha |A_2|^2 A_2 \right\} + \mathcal{O}(\varepsilon^2), \end{aligned} \quad (34)$$

from which we have a naive RG map up to $\mathcal{O}(\varepsilon)$

$$A_j^n = A_j + \varepsilon \frac{i\tau^2}{2 \sin \theta} \left(\nu L_j A_j - 3\alpha |A_j^n|^2 A_j^n \right), \quad (j = 1, 2) \quad (35)$$

where, $L_j A_j$ is defined by Eq. (19). The naive RG map (35) should be regularized by means the symplectic integration method. Then, we get a regularized RG map:

$$\left(1 - iTL_j \right) A_j^{n+1} = \left(1 + iTL_j \right) \exp \left(iQ |A_j^n|^2 \right) A_j, \quad (36)$$

which has the following matrix form useful to numerical calculations:

$$\begin{pmatrix} 1+iT & -iT \\ -iT & 1+iT \end{pmatrix} \begin{pmatrix} A_1^{n+1} \\ A_2^{n+1} \end{pmatrix} = \begin{pmatrix} 1-iT & +iT \\ +iT & 1-iT \end{pmatrix} \begin{pmatrix} B_1^n \\ B_2^n \end{pmatrix}. \quad (37)$$

By inverting the matrix in Eq.(37), we have

$$\begin{pmatrix} A_1^{n+1} \\ A_2^{n+1} \end{pmatrix} = \frac{1-2iT}{1+4T^2} \begin{pmatrix} 1 & 2iT \\ 2iT & 1 \end{pmatrix} \begin{pmatrix} B_1^n \\ B_2^n \end{pmatrix}.$$

Appendix C: Continuous-time RG equation with two sites

In order to picture a homoclinic manifold resulting from the modulational instability clearly, let us analyze a continuous-time RG equation with two sites, which is integrable. In this case, the continuous-time RG equation has the following form (see Eq.(33))

$$\begin{aligned} \frac{d\tilde{A}_1}{dt} &= \frac{i\varepsilon}{2\Omega} \left\{ \nu(\tilde{A}_2 - \tilde{A}_1) - 3\alpha|\tilde{A}_1|^2\tilde{A}_1 \right\}, \\ \frac{d\tilde{A}_2}{dt} &= \frac{i\varepsilon}{2\Omega} \left\{ \nu(\tilde{A}_1 - \tilde{A}_2) - 3\alpha|\tilde{A}_2|^2\tilde{A}_2 \right\}, \end{aligned}$$

Since the regime where the modulational instability occurs is of interest, we suppose $\nu = -|\nu| < 0$ and $\alpha > 0$ and introduce new variables:

$$t' = |\nu| \frac{\varepsilon}{2\Omega} t, \quad Q_j = \sqrt{\frac{3\alpha}{|\nu|}} \exp\left\{ \frac{i\nu\varepsilon t}{2\Omega} \right\} \tilde{A}_j. \quad (j = 1, 2)$$

Then, we have

$$\begin{aligned} \frac{dQ_1}{dt'} &= -i(Q_2 + |Q_1|^2 Q_1) = \frac{\partial \mathcal{H}}{\partial Q_1^*}, & \frac{dQ_1^*}{dt'} &= -\frac{\partial \mathcal{H}}{\partial Q_1}, \\ \frac{dQ_2}{dt'} &= -i(Q_1 + |Q_2|^2 Q_2) = \frac{\partial \mathcal{H}}{\partial Q_2^*}, & \frac{dQ_2^*}{dt'} &= -\frac{\partial \mathcal{H}}{\partial Q_2}, \\ \mathcal{H} &= -i \left\{ Q_1^* Q_2 + Q_1 Q_2^* + (|Q_1|^4 + |Q_2|^4)/2 \right\}, \end{aligned}$$

which has a uniformly oscillating solution

$$Q_j(t') = Q_0(0) \exp\left\{ -i(1 + |Q_0(0)|^2) t' \right\} \quad (j = 1, 2).$$

To construct a homoclinic manifold of the unstable periodic solution, we transform Q_j into a_j as

$$Q_j(t') \equiv a_j(t') \exp \left\{ -i(1 + |Q_0(0)|^2) t' \right\}.$$

and have

$$\frac{da_1}{dt'} = -i \left[\left\{ |a_1|^2 - (1 + |Q_0|^2) \right\} a_1 + a_2 \right], \quad (38)$$

$$\frac{da_2}{dt'} = -i \left[\left\{ |a_2|^2 - (1 + |Q_0|^2) \right\} a_2 + a_1 \right]. \quad (39)$$

This system has two conserved quantities, i.e. the Hamiltonian and $|a_1|^2 + |a_2|^2$, and is integrable. After some manipulations of Eqs.(38) and (39), we obtain an explicit expression of homoclinic manifold:

$$\begin{aligned} a_1 &= b\sqrt{1 + \Gamma} \exp\{i(\Theta + \Delta)/2\}, \\ a_2 &= b\sqrt{1 - \Gamma} \exp\{i(\Theta - \Delta)/2\}, \end{aligned}$$

and

$$\begin{aligned} \Gamma(t') &= \frac{2}{b^2} \sqrt{b^2 - 1} \operatorname{sech}(-2\sqrt{b^2 - 1}t'), \\ \Delta(t') &= \operatorname{Cos}^{-1} \left(\frac{1 - b^2\Gamma^2/2}{\sqrt{1 - \Gamma^2}} \right), \\ \Theta(t') &= -\frac{1 - b^2/2}{b^2 - 1} \frac{B}{\sqrt{1 - B^2}} \operatorname{Tan}^{-1} \left\{ \frac{B}{1 - B^2} \tanh \left(2\sqrt{b^2 - 1}t' \right) \right\} + \operatorname{const.}, \end{aligned}$$

where $B \equiv 2\sqrt{b^2 - 1}/b^2$ and $b \equiv |Q_0(0)| > 1$.

Appendix D: Modulational instability for the case of odd sites

In this section, we provide instability conditions for a uniformly oscillating solution of the reduced map (14) with odd sites by means of the Fourier analysis [13]. We substitute Eq. (23) into Eq. (14), where perturbation is set as

$$\mu_j^n = \sum_a \hat{\mu}_a^j \exp \left(i \frac{2\pi}{N} a j \right), \quad (40)$$

$$a \in \left\{ -\frac{N-1}{2}, -\frac{N-1}{2} + 1, \dots, 0, \dots, \frac{N-1}{2} - 1, \frac{N-1}{2} \right\},$$

and N is an odd number ($N \geq 3$). Assuming the periodic boundary condition $\mu_{j+N}^n = \mu_j^n$, we have a linearized equation for μ_j^n .

$$\begin{pmatrix} \hat{\mu}_j^{n+1} \\ \hat{\mu}_j^{n+1*} \end{pmatrix} = \begin{pmatrix} d_a(1+iQ|A^0|^2) & d_a iQ|A^0|^2 \\ d_a^{-1}(-iQ|A^0|^2) & d_a^{-1}(1-iQ|A^0|^2) \end{pmatrix} \begin{pmatrix} \hat{\mu}_a^n \\ \hat{\mu}_a^{n*} \end{pmatrix}, \quad (41)$$

where $a \neq 0$ and

$$d_a \equiv \frac{1 - 4iT \sin^2(\pi a/N)}{1 + 4iT \sin^2(\pi a/N)}.$$

The eigenvalues of Eq. (41) are

$$\lambda_{a\pm} = \beta_a \pm \sqrt{\beta_a^2 - 1}, \quad (42)$$

where

$$\beta_a \equiv \frac{1 + 8QT|A^0|^2 \sin^2(\pi a/N) - \left(4T \sin^2(\pi a/N)\right)^2}{1 + \left(4T \sin^2(\pi a/N)\right)^2} \in \mathbf{R}.$$

Note that $\lambda_{a+}\lambda_{a-} = 1$. The uniformly oscillating solution is destabilized when

$$\beta_a > 1 \quad \text{or} \quad \beta_a < 1,$$

that is

$$|A^0|^2 > \frac{4T \sin^2(\pi a/N)}{Q}, \quad \text{or} \quad |A^0|^2 < -\frac{1}{4QT \sin^2(\pi a/N)}. \quad (43)$$

The instability condition (43) and the spectrum of eigenvalues (42) give information about dimensions of invariant manifolds around the uniformly oscillating solution (a torus) characterized by $|A^0|$.

References

- [1] V.G. Gelfreich and D.K. Sharomov, Phys. Lett. **A197** (1995), 139.
- [2] Y. Hirata, K. Nozaki and T. Konishi, Prog. Theor. Phys. **101** (1999), 1181.

- [3] Y. Hirata, K. Nozaki and T. Konishi, Prog. Theor. Phys. **102** (1999), 701.
- [4] V. I. Arnold, Sov. Math. Dokl. **5** (1964), 581. *or* V. I. Arnold and A. Avez, “Ergodic Problems in classical Mechanics”, *Benjamin-Cummings Reading, Massachusetts*.
- [5] S. Goto and K. Nozaki, Prog. Theor. Phys. **102** (1999), 953.
- [6] L. Y. Chen, N. Goldenfeld and Y. Oono, Phys. Rev. **E54** (1996), 376.
- [7] S. Goto, Y. Masutomi, and K. Nozaki, Prog. Theor. Phys. **102** (1999), 471.
- [8] S. Goto and K. Nozaki, Prog. Theor. Phys. **105** (2001), 99.
- [9] S. Goto and K. Nozaki, J. Phys. Soc. Jpn. **70** (2001), 49.
- [10] M. J. Ablowitz, B. M. Herbst and C. M. Schober, Physica **A 228** (1996), 212.
- [11] David W. McLaughlin and Constance M. Schober, Physica **D57** (1992), 447.
- [12] B.M. Herbst, F. Varadi and M.J. Ablowitz, Mathematics and Computers in simulation **37** (1994), 353.
- [13] J. A. C. Weideman and B. M. Herbst, SIAM. J. Numer. Anal. **23** (1986), 485.

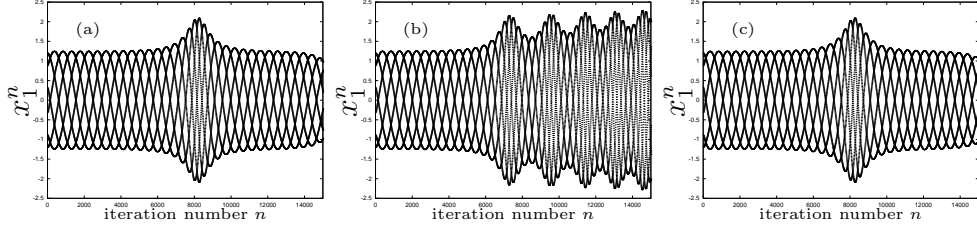


Figure 1: The time sequences of three-site model. (a) trajectory constructed from the original map, (b) the naive RG map and (c) the regularized RG map.

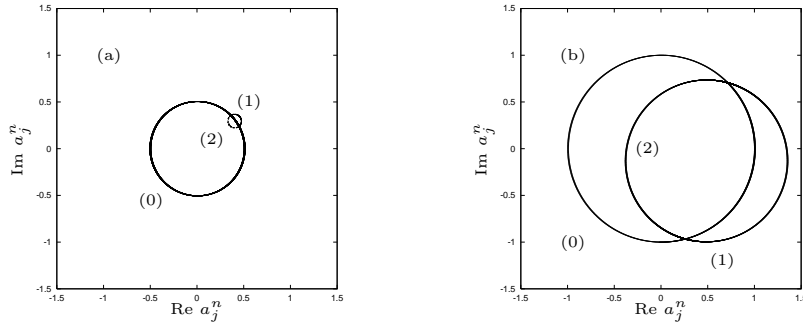


Figure 2: (a) The phase space of the two-site model near the hyperbolic torus for $|A^0| = |A_c| + 0.005$. Here (0) corresponds to a uniform solution $A_j^n = A^0 \exp(iQ|A^0|^2 n)$, and (1), (2) correspond to a_1^n and a_2^n , respectively. The initial condition is as follows : $\text{Re}A_1^0 = |A^0|/\sqrt{2} + 0.0002$, $\text{Re}A_2^0 = |A^0|/\sqrt{2} + 0.0001$, $\text{Im}A_1^0 = |A^0|/\sqrt{2} + 0.0$, $\text{Im}A_2^0 = |A^0|/\sqrt{2} + 0.0$. (b) The initial conditions are same as (a) when $|A^0| = |A_c| + 0.5$.

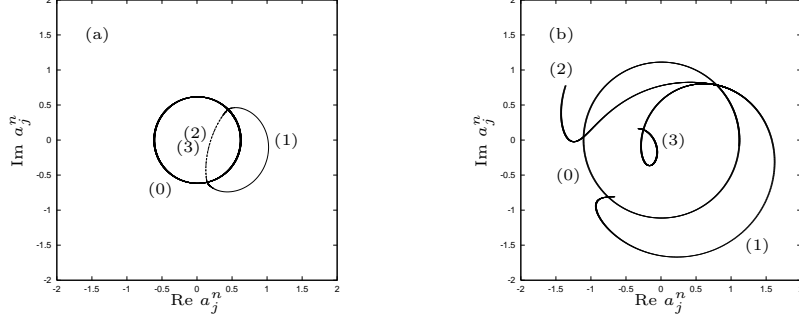


Figure 3: (a) The phase space of the three-site model near the hyperbolic torus for $|A^0| = |A_c| + 0.005$. Here (0) corresponds to a uniform solution $A_j^n = A^0 \exp(iQ|A^0|^2 n)$, and (1), \dots , (3) correspond to a_1^n, \dots, a_3^n , respectively. The initial condition is as follows : $\text{Re}A_1^0 = |A^0|/\sqrt{2} + 0.0003$, $\text{Re}A_2^0 = |A^0|/\sqrt{2} + 0.0002$, $\text{Re}A_3^0 = |A^0|/\sqrt{2} + 0.0001$, $\text{Im}A_1^0 = |A^0|/\sqrt{2} + 0.0$, $\text{Im}A_2^0 = |A^0|/\sqrt{2} + 0.0$, $\text{Im}A_3^0 = |A^0|/\sqrt{2} + 0.0$. (b) The initial conditions are same as (a) when $|A^0| = |A_c| + 0.5$.

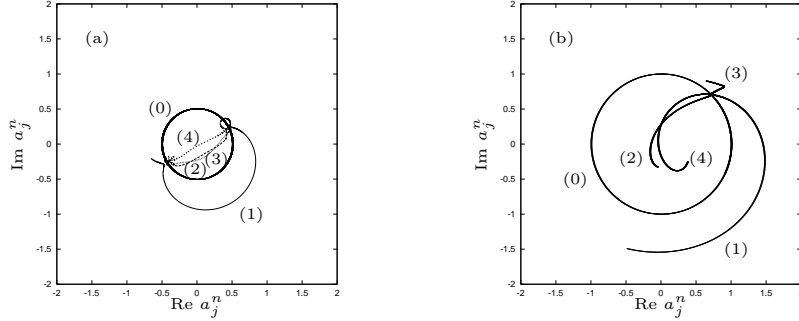


Figure 4: (a) The phase space of the four-site model near the hyperbolic torus for $|A^0| = |A_c| + 0.005$. Here (0) corresponds to a uniform solution $A_j^n = A^0 \exp(iQ|A^0|^2 n)$, and (1), \dots , (4) correspond to a_1^n, \dots, a_4^n , respectively. The initial condition is as follows : $\text{Re}A_1^0 = |A^0|/\sqrt{2} + 0.0004$, $\text{Re}A_2^0 = |A^0|/\sqrt{2} + 0.0003$, $\text{Re}A_3^0 = |A^0|/\sqrt{2} + 0.0002$, $\text{Re}A_4^0 = |A^0|/\sqrt{2} + 0.0001$, $\text{Im}A_1^0 = |A^0|/\sqrt{2} + 0.0$, $\text{Im}A_2^0 = |A^0|/\sqrt{2} + 0.0$, $\text{Im}A_3^0 = |A^0|/\sqrt{2} + 0.0$, $\text{Im}A_4^0 = |A^0|/\sqrt{2} + 0.0$. (b) The initial conditions are same as (a) when $|A^0| = |A_c| + 0.5$.

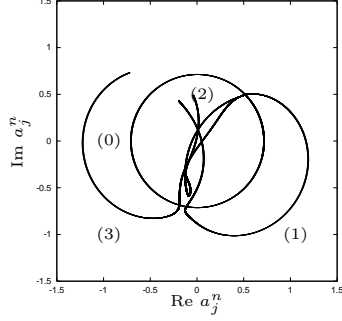


Figure 5: The phase space of the three-site model near the hyperbolic torus for $|A^0| = |A_c| + 0.1$. Here (0) corresponds to a uniform solution $A_j^n = A^0 \exp(iQ|A^0|^2 n)$, and (1), \dots , (3) correspond to a_1^n, \dots, a_3^n , respectively. The initial condition is as follows : $\text{Re}A_1^0 = |A^0|/\sqrt{2} + 0.003$, $\text{Re}A_2^0 = |A^0|/\sqrt{2} + 0.002$, $\text{Re}A_3^0 = |A^0|/\sqrt{2} + 0.001$, $\text{Im}A_1^0 = |A^0|/\sqrt{2} + 0.0$, $\text{Im}A_2^0 = |A^0|/\sqrt{2} + 0.0$, $\text{Im}A_3^0 = |A^0|/\sqrt{2} + 0.0$.

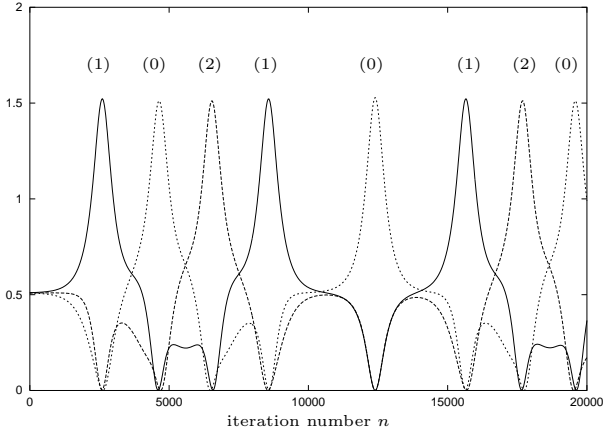


Figure 6: The time sequences of $|a_j^n|^2$ of the three-site model near the hyperbolic torus for $|A^0| = |A_c| + 0.1$. Here (1), (2) and (0) correspond to $|a_1^n|^2$, $|a_2^n|^2$ and $|a_3^n|^2$, respectively. The orbit is characterized by the sequence of site-numbers $10210120\dots$. The initial condition is as follows : $\text{Re}A_1^0 = |A^0|/\sqrt{2} + 0.003$, $\text{Re}A_2^0 = |A^0|/\sqrt{2} + 0.002$, $\text{Re}A_3^0 = |A^0|/\sqrt{2} + 0.001$, $\text{Im}A_1^0 = |A^0|/\sqrt{2} + 0.0$, $\text{Im}A_2^0 = |A^0|/\sqrt{2} + 0.0$, $\text{Im}A_3^0 = |A^0|/\sqrt{2} + 0.0$.

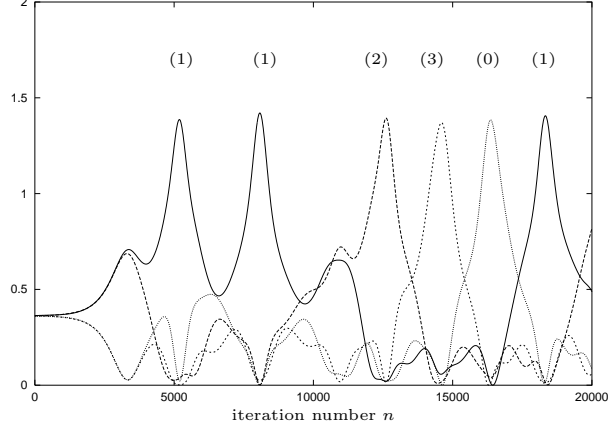


Figure 7: The time sequences of $|a_j^n|^2$ of the four-site model near the hyperbolic torus for $|A^0| = |A_c| + 0.1$. Here (1), (2), (3) and (0) correspond to $|a_1^n|^2$, $|a_2^n|^2$, $|a_3^n|^2$ and $|a_4^n|^2$, respectively. The orbit is characterized by the sequence of site-numbers 112301... The initial condition is as follows : $\text{Re}A_1^0 = |A^0|/\sqrt{2} + 0.004$, $\text{Re}A_2^0 = |A^0|/\sqrt{2} + 0.003$, $\text{Re}A_3^0 = |A^0|/\sqrt{2} + 0.002$, $\text{Re}A_4^0 = |A^0|/\sqrt{2} + 0.001$, $\text{Im}A_1^0 = |A^0|/\sqrt{2} + 0.0$, $\text{Im}A_2^0 = |A^0|/\sqrt{2} + 0.0$, $\text{Im}A_3^0 = |A^0|/\sqrt{2} + 0.0$, $\text{Im}A_4^0 = |A^0|/\sqrt{2} + 0.0$,

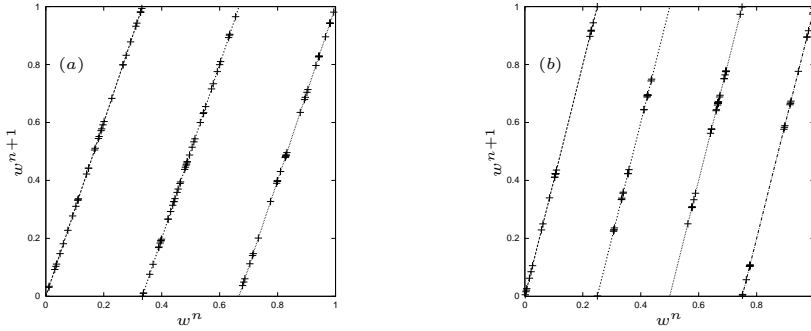


Figure 8: (a) The Bernoulli sequences of the three-site model near the hyperbolic torus for $|A^0| = |A_c| + 0.1$. (b) same as (a) for four-site model.